Sensors and Materials, Vol. 31, No. 12 (2019) 3999–4011
MYU Tokyo

S & M 2065

Hybrid Peak-to-average-power-ratio Reduction Method Based on Filter Bank Multicarrier in Wireless Sensor Networks

Song Liu,[1*] Yue Li,[1] and Jianqiang Wang[2]

[1]North China Electric Power University, Beijing 102206, China
[2]Inner Mongolia Power (Group) Co., Ltd., Inner Mongolia 010000, China

(Received March 22, 2019; accepted November 5, 2019)

Keywords: peak-to-average-power ratio (PAPR), filter bank multicarrier (FBMC), clipping and filtering, Vandermonde-like matrix (VLM), wireless sensor networks (WSNs)

Filter bank multicarrier (FBMC) technology is considered a suitable solution for replacing orthogonal frequency division multiplexing (OFDM) technology for the transmission of the fifth-generation wireless system (5G) multicarrier. In this study, we investigate the problem of a high peak-to-average-power ratio (PAPR) of FBMC in wireless sensor networks (WSNs). To solve the problem of imaginary interference in the FBMC system, we use an auxiliary pilot. Then, on the basis of the pilot-assisted FBMC system, a hybrid method of the Vandermonde-like matrix (VLM) and clipping with filtering is applied to reduce the PAPR. The input data is precoded by the VLM of Chebyshev polynomials to reduce the autocorrelation of the input signal. Then, the signal is sent to the clipping and filtering module to suppress the PAPR of the FBMC signal further. The pilot-assisted FBMC was applied to the multipath channel model. The performance was evaluated using the PAPR and bit error rate (BER) curves. The simulation results indicate that the hybrid method can improve the PAPR suppression performance of the FBMC system compared with the precoding method or the clipping and filtering method alone. From the results, we can also see that the hybrid method improves the BER performance.

1. Introduction

Wireless sensor networks (WSNs) are one of the supporting technologies of the Internet of things industry, which is of great significance for promoting economic development and scientific and technological progress. Because of its rapid deployment, convenient networking, and unrestricted nodes, it is widely used in battlefield detection, disaster rescue, and environmental perception. Therefore, WSNs have become a hot topic of academic and industrial research. WSNs transmit information to users through sensor nodes; this requires the use of sensing, collection, embedded distribution, and communication technologies to complete information-related collection, processing, and transmission tasks. However, owing to the dense distribution and large quantity of WSNs, it is easy to be affected by problems such as uncertain

*Corresponding author: e-mail: liusong@ncepu.edu.cn
https://doi.org/10.18494/SAM.2019.2387

ISSN 0914-4935

topological structure, insufficient energy consumption guarantee, and limited computing and storage capacity, among which, the cost and energy consumption of nodes are the key factors restricting the extensive application and promotion of nodes.[1]

Currently, there are two IEEE standards for information transmission in WSNs. IEEE802 is designed for low-speed wireless personal LAN, and the IEEE802 standard, which provides the ultrawide-band (UWB) wireless personal area network (WPAN) physical layer in the 7 GHz band between 3 and 10 GHz to WSNs, allows multiple signals to jointly occupy the entire bandwidth. Because of the existence of different subcarriers in the multiband, the subcarriers can use different data modulation modes, and filter bank multicarrier (FBMC) technology is suitable for the over-bandwidth wireless communication system.[2]

In future wired and wireless communication standards,[3,4] FBMC will be a promising technology that avoids the use of redundant samples as the cyclic prefix (CP). By using the FBMC system, spectral efficiency and robustness to synchronization requirements can be improved. Moreover, in a noise environment, such as in a powerline channel, FBMC has a stronger robustness.[5]

One problem with FBMC is imaginary interference. To deal with the problem, Javaudin *et al.*[6] used one symbol per pilot, the so-called auxiliary pilot symbol, to cancel the imaginary interference.[7] The main disadvantage of this method is the power offset. To solve this problem, Nissel and Rupp[8] used two auxiliary symbols per pilot to reduce the power offset from 4.3 to 0.8 and to increase the achievable capacity for low signal-to-noise ratio (SNR) values by approximately 5%. Therefore, we study the peak-to-average-power ratio (PAPR) in the FBMC system with an auxiliary pilot, which we refer to as the pilot-assisted FBMC system.

One of the biggest problems, however, is the PAPR of the transmitted FBMC signal, as this large peak can cause a significant performance degradation when the signal passes through a nonlinear high-power amplifier (HPA). The nonlinearity of HAP leads to in-band distortion, resulting in increased bit error rate (BER) and adjacent channel interference owing to out-of-band (OOB) radiation.[9] For this reason, several methods, such as selective level mapping (SLM),[10] partial transmit sequence,[11] square-rooting companding, absolute exponential companding, tone reservation (TR), clipping, and active constellation extension,[9,12,13] have been proposed to reduce the PAPR of the FBMC signal.

Because of the overlapping signal structure of the FBMC system, the direct application of the above scheme originally adjusted for orthogonal frequency division multiplexing (OFDM) is infeasible. To adapt it to the signal structure of FBMC, some signal processing operations must be introduced into these PAPR reduction schemes. There are some works on the PAPR reduction of FBMC systems in the literature. In Ref. 14, Hrasnica *et al.* described the use of the sliding window algorithm to improve the TR scheme and used it for the PAPR reduction of FBMC signals. This advanced scheme, known as sliding window tone retention (SWTR), eliminates the peak value of the FBMC signal in the window by using a series of continuous blocks of peak scaling tones. SW-TR can properly reduce the PAPR of FBMC signals. Zimmermann and Dostert[15] and Krongold and Jones[16] proposed overlapping SLM to reduce the PAPR of OFDM signals. Dongjun and Choi proposed a low-PAPR scheme and resolved a pending issue of FBMC, i.e., OOB spectrum regrowth due to HPA nonlinearity.[17]

In this paper, the Vandermonde-like matrix (VLM) and clipping with filtering-based PAPR-reduction schemes aided to reduce the PAPR of FBMC signals are presented. The pilot-assisted FBMC was transmitted to the PLC channel model and the performance was evaluated using PAPR and BER curves.

The paper is organized as follows. In Sect. 2, the main features of FBMC and PLC channel models are introduced, and the form of FBMC receiving signal transmitted through a multipath channel is derived. In Sect. 3, the PAPR reduction methods based on the pilot-assisted FBMC, including clipping, filtering, VLM, and their combinations are discussed. In Sect. 4, simulation and experimental results are given. Finally, we summarize this paper in Sect. 5.

2. System Model

2.1 FBMC system

The implementation structure of FBMC is shown in Fig. 1. In the literature, this structure has often been referred to as OFDM-OQAM, where OQAM stands for offset quadrature amplitude modulation (QAM).

FBMC filters each subcarrier modulated signal in a multicarrier system. The prototype filter is the one used for the zero-frequency carrier and is the basis of the other subcarrier filters. The filters are characterized by the overlapping factor K, which is the number of multicarrier symbols that overlap in the time domain. The prototype filter order can be chosen as $2 \times K - 1$ where $K = 2$, 3, or 4 and is selected as per PHYDYAS project.

The current FBMC implementation uses frequency spreading and an $N \times K$-long inverse fast Fourier transform (IFFT) with symbols overlapped with a delay of $N/2$, where N is the number of subcarriers. This design choice makes it easy to analyze FBMC and compare the results with those of other modulation methods.

To achieve a full capacity, OQAM processing is employed. The real and imaginary parts of a complex data symbol are not transmitted simultaneously, as the imaginary part is delayed by half the symbol duration.

The modulation is achieved digitally using an IFFT. P/S and S/P represent parallel-to-serial and serial-to-parallel conversions, respectively.

In the FBMC transmission system, a series of data signals are transformed firstly and concatenated through source and channel codes, and then mapped into a certain space to

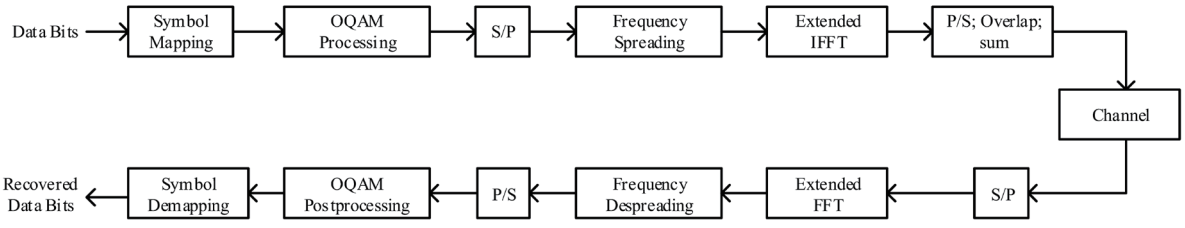

Fig. 1. Implementation structure of FBMC.

improve the transmission efficiency of information bits. Complex number sequences are divided into real and imaginary parts. In the FBMC system, OQAM is used to preprocess symbols of the real and imaginary parts. The preprocessed symbols are then modulated by prototype filters, applying filter bank multicarrier technology, and superimposed to the channel in the time domain. With the help of the IFFT algorithm, the modulation of multicarrier technology can be realized rapidly. At the receiving end, a set of symmetric prototype filters are also used, which have exactly the same performance as the original filter banks at the sending end.

The processing includes matched filtering followed by OQAM separation to form the received data symbols. These data symbols are demapped into bits and the resultant BER is determined. In the presence of a channel, linear multitap equalizers may be used to mitigate the effects of frequency-selective fading. Demodulation is performed by a fast Fourier transform (FFT).

Mathematically, the transmitter signal $x(t)$ of the multicarrier system in the time domain can be expressed as

$$x(t) = \sum_{n=-\infty}^{+\infty} \sum_{m=0}^{M-1} a_{m,n} g_{m,n}(t), \tag{1}$$

where M represents the number of subcarriers and $a_{m,n}$ denotes the transmitted symbol at the subcarrier position m and time position n. The transmitted basis pulse $g_{m,n}(t)$ in Eq. (1) is defined as

$$g_{m,n}(t) = g(t - n\tau_0) e^{j2\pi m F_0 t} e^{j\frac{\pi}{2}(n+m)}, \tag{2}$$

where $g_{m,n}(t)$ is the time and frequency-shifted version of the prototype filter $g(t)$ with τ_0 denoting the time spacing and $1/F_0$ the frequency spacing. $e^{j\frac{\pi}{2}(n+m)}$ is the adjustment of the phase, which ensures real orthogonality between the systems.

2.2 Multipath channel model

In this paper, we use the practical multipath channel model introduced by Zimmermann and Dostert,[15] which is suitable for describing the transmission behavior of power line channels. On the basis of the actual measurement of the actual powerline network, the model is given by the channel transfer function[12]

$$H(f) = \sum_{i=1}^{I} \underbrace{g_i}_{\text{weighting factor}} \cdot \underbrace{e^{-(a_0 + a_1 f^{\beta}) d_i}}_{\text{attenuation portion}} \cdot \underbrace{e^{-j2\pi f \left(\frac{d_i}{v_p}\right)}}_{\text{delay portion}}, \tag{3}$$

where g_i is the weighting factor representing the product of the reflection and transmission

factors for each path i. The attenuation parameters a_0 (offset of attenuation), a_1 (increase in attenuation), and β (exponent of attenuation) are derived from the measured frequency response.[12] d_i represents the length of the cable. v_p is the phase velocity.

2.3 FBMC in multipath channel model

After transmission over the channel, the received symbols $r(t)$ of the FBMC can be expressed as

$$r(t) = h(t) \otimes x(t) = \int_0^{\Delta} h(t,\tau) x(t-\tau) d\tau \,, \tag{4}$$

where $h(t, \tau)$ represents the impulse response of the multipath channel model. Δ represents the maximum delay extension of the channel. Substituting Eq. (1) into Eq. (4) gives

$$\begin{aligned} r(t) &= \sum_{n=-\infty}^{+\infty} \sum_{m=0}^{N-1} a_{m,n} \int_0^{\Delta} h(t,\tau) g_{m,n}(t-\tau) d\tau \\ &= \sum_{n=-\infty}^{+\infty} \sum_{m=0}^{N-1} a_{m,n} e^{j\frac{\pi}{2}(n+m)} e^{j2\pi m v_0 t} \cdot \int_0^{\Delta} h(t,\tau) g(t-\tau-n\tau_0) e^{-j2\pi m v_0 \tau} d\tau \,. \end{aligned} \tag{5}$$

Assuming that the delay spread Δ of the multipath channel is much smaller than one symbol period, it can be approximated in the time span of $0 \le \tau \le \Delta$:

$$g(t-\tau-n\tau_0) \approx g(t-n\tau_0). \tag{6}$$

In this case, Eq. (6) can be simplified as

$$r(t) = \sum_{n=-\infty}^{+\infty} \sum_{m=0}^{N-1} a_{m,n} e^{j\frac{\pi}{2}(n+m)} e^{j2\pi m v_0 t} g(t-n\tau_0) H_m(t) \,, \tag{7}$$

where $H_m(t) = \int_0^{\Delta} h(t,\tau) e^{-j2\pi m v_0 \tau} d\tau$ represents the channel frequency domain response of the mth subchannel at time t. For slow time-varying multipath channels, the fading experienced by data on the same subcarrier between different FBMC symbols can be considered to be the same; then, $H_m(t) = H_m$, and hence

$$r(t) = \sum_{n=-\infty}^{+\infty} \sum_{m=0}^{N-1} a_{m,n} g_{m,n} H_m \,. \tag{8}$$

After the received signal passes through the receive filter, the demodulated signal at point (n_0, m_0) can be expressed as

$$r_{m_0,n_0} = a_{m_0,n_0} H_{m_0} + \sum_{n=-\infty}^{+\infty} \sum_{m=0}^{N-1} a_{m,n} H_m \left\langle g_{m,n}(t),\, g_{m_0,n_0}(t) \right\rangle . \tag{9}$$

3. Hybrid PAPR Reduction Method

3.1 Definition of PAPR in FBMC system

In general, the ratio between the maximum peak power and the average power over a period of time is called the PAPR. For a continuous time baseband signal $x(t)$, PAPR within a transmission period t is defined as

$$PAPR_{x(t)} = \frac{\max\limits_{0 \le t \le T} |\, x(t) \,|^2}{\frac{1}{T_0} \int_0^T |\, x(t) \,|^2 \, dt} . \tag{10}$$

Most PAPR reduction schemes are performed on frequency domain signals, so we need to sample the FBMC signal in the continuous time domain. The ordinary Nyquist rate sampling will lose some peak values, so we need to use oversampling technology in the actual operation. The PAPR expression of the baseband modulation discrete-time signal $x(n)$ is

$$PAPR_{x(n)} = 10 \lg \frac{\max\left(\left| x(n) \right|^2 \right)}{E\left(\left| x(n) \right|^2 \right)} . \tag{11}$$

The complementary cumulative distribution function (CCDF) is a common method of measuring and calculating the multicarrier PAPR. CCDF is defined as the probability that the PAPR of the mth modulation symbol exceeds a given threshold, and its expression is

$$CCDF\left[PAPR_{x(m)} \right] = \Pr\left(PAPR_{x(m)} > \gamma \right) . \tag{12}$$

In the following sections, we use the CCDF function to measure the PAPR distribution of the FBMC system.

3.2 Clipping and filtering

Figure 2 shows a block diagram of a PAPR reduction scheme including clipping and filtering, where L is the oversampling factor and N is the number of subcarriers. In this scheme, the L-times-oversampled discrete-time signal $x'[m]$ is generated from the IFFT and is then modulated with the carrier frequency f_c to yield a passband signal $x^p\left[m\right]$. Let $x_c^p\left[m\right]$ denote the clipped version of $x^p[m]$, which is expressed as

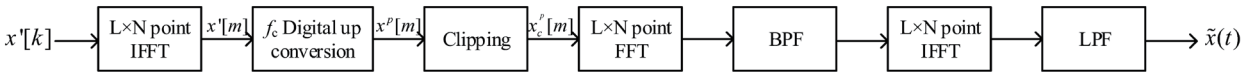

Fig. 2. Block diagram of a PAPR reduction scheme with clipping and filtering.

$$x_c^p[m]=\begin{cases}-A & x^p[m]\le -A\\ x^p[m] & \left|x^p[m]<A\right|\\ A & x^p[m]\ge -A\end{cases}, \tag{13}$$

where A is the prespecified clipping level. Let us define the clipping ratio (CR) as the clipping level normalized by the RMS value of the FBMC signal such that

$$CR=\frac{A}{\sigma}. \tag{14}$$

It is known that $\sigma=\sqrt{N}$ and $\sigma=\sqrt{N/2}$ in the baseband and passband FBMC signals with N subcarriers, respectively.

Using clipping to suppress PAPR will cause in-band noise and increased OOB radiation owing to distortion caused by the direct limitation of the signal amplitude, thus reducing the BER performance of the system. Because clipping can cause OOB spectrum dispersion, clipping and filtering can eliminate OOB interference by filtering the limited data and hence improve the system BER performance of the system.

3.3 Hybrid PAPR suppression method

The input data is precoded by the VLM of the Chebyshev polynomial to reduce the autocorrelation of the input signal. Then, the signal is sent to the clipping and filtering module to suppress the PAPR of the signal further.

Suppose a_1, a_2, …, a_n are n real or complex numbers, and $T_k(x)$ (k = 0, 1, …, n − 1) is a polynomial of degree k and satisfies the following recursive relation:

$$\begin{cases}T_0(x)=1\\ T_1(x)=\lambda_1(x-\alpha_1)T_0(x)\\ T_k(x)=\lambda_k(x-\alpha_k)T_{k-1}(x)-\beta_k T_{k-2}(x)\ \ (k\ge 2)\\ \quad \lambda_k\ne 0\ \ (k=1,2,...,n-1)\end{cases}. \tag{15}$$

The n-order square matrix $\boldsymbol{B}$ composed of $T_k(x)$ is called the VLM.

$$\boldsymbol{B}=\begin{bmatrix} T_0(\alpha_1) & T_0(\alpha_2) & \cdots & T_0(\alpha_n) \\ T_1(\alpha_1) & T_1(\alpha_2) & \cdots & T_1(\alpha_n) \\ \vdots & \vdots & \ddots & \vdots \\ T_{n-1}(\alpha_1) & T_{n-1}(\alpha_2) & \cdots & T_{n-1}(\alpha_n) \end{bmatrix} \tag{16}$$

When $T_k(x) = x^k$ (k = 0, 1, ..., n − 1), λ_k = 1, α_k = 0, and β_k = 0, $\boldsymbol{B}$ is the Vandermonde matrix. In the VLM, the polynomial $T_k(x)$ is called the Chebyshev polynomial, that is, $T_k(x)$ = cos($k$arccos(x)) satisfies

$$\begin{cases} T_0(x)=1 \\ T_1(x)=x \\ T_k(x)=2xT_{k-1}(x)-T_{k-2}(x)\ \ (k\geq 2). \end{cases} \tag{17}$$

Let $x_j=\cos\dfrac{(j-1)\pi}{n-1}$ or $x_j=\cos\dfrac{(j-1/2)\pi}{n}$, where $x_j=\cos\dfrac{(j-1)\pi}{n-1}$ is the pole of $T_{n-1}(x)$ and $x_j=\cos\dfrac{(j-1/2)\pi}{n}$ is the zero of $T_{n-1}(x)$. Then, when the nodes are respectively taken as the poles and zeros of the Chebyshev polynomial, the Chebyshev–Vandermonde matrices $\boldsymbol{C}$ and $\boldsymbol{D}$ are respectively

$$\begin{cases} \boldsymbol{C}=\cos\dfrac{(i-1)(j-1)\pi}{n-1},\ \alpha_j=\cos\dfrac{(j-1)\pi}{n-1} \\ \boldsymbol{D}=\cos\dfrac{(i-1)(j-1/2)\pi}{n},\ \alpha_j=\cos\dfrac{(j-1/2)\pi}{n}. \end{cases} \tag{18}$$

Assuming that the parallel input signal after encoding and modulation is X and x is obtained after the IFFT, the instantaneous power is

$$\begin{aligned} P_n &= \left|x_n\right|^2 = x_n\cdot x_n^* \\ &= \frac{1}{N}\sum_{m=0}^{N-1}\sum_{k=0}^{N-1} X_k X_m^* \exp\left[j\frac{2\pi}{N}(k-m)n\right] \\ &= \frac{1}{N}\left\{N+2\Re\left[\sum_{m=0}^{N-2}\sum_{k=m+1}^{N-1} X_k X_m^* \exp\left[j\frac{2\pi}{N}(k-m)n\right]\right]\right\}, \\ &= 1+\frac{2}{N}\Re\left\{\sum_{k=1}^{N-1}\exp\left(j\frac{2\pi}{N}kn\right)\sum_{m=0}^{N-k-1} X_{k+m}X_m^*\right\} \\ &\leq 1+\frac{2}{N}\sum_{k=1}^{N-1}\left|\sum_{m=0}^{N-k-1} X_{k+m}X_m^*\right| = 1+\frac{2}{N}\sum_{k=1}^{N-1}\left|\lambda(k)\right| \end{aligned} \tag{19}$$

where

$$\lambda(k) = \sum_{m=0}^{N-k-1} X_{k+m} X_m^* . \tag{20}$$

$\lambda(k)$ is the aperiodic autocorrelation function of input signal X.

The average power of the signal is fixed. Let the average power $P_{av} = E\{|x_n|^2\}$; then, the PAPR is

$$PAPR = \frac{P_n}{P_{av}} \le \frac{1}{P_{av}} \left(1 + \frac{2}{N} \sum_{k=1}^{N-1} \left| \lambda(k) \right| \right). \tag{21}$$

Chebyshev polynomials have orthogonality,[18] which can reduce the autocorrelation of input data by linear precoding input signal sequences through the VLM composed by them. According to Eq. (21), PAPR is related to the input signal's aperiodic autocorrelation function. The smaller the sum of the modules of the signal's aperiodic autocorrelation function is, the smaller PAPR will be after the signal is transformed into the time domain. Therefore, the input signal can be precoded by the Chebyshev–Vandermonde matrix to reduce the autocorrelation of the input signal and thus reduce the PAPR of the FBMC signal.

The specific process of the hybrid method is as follows. At the transmitting end of the system, after encoding, modulating, and concatenating the input serial data, linear precoding is carried out using the VLM of the Chebyshev polynomial, and the time domain data is obtained by oversampling and IFFT. After limiting the time domain data in accordance with the set limiting ratio, the frequency domain data is obtained through the FFT. The IFFT is carried out again to obtain the time domain data. Finally, the data is sent after parallel string conversion, the insertion of the CP, digital-to-analog conversion, and other processes. The receivers in the system undergo a corresponding process. The received signal removes the CP after the analog-to-digital conversion. After series-to-parallel conversion, the frequency domain data is obtained by FFT. Then, the frequency domain data is decoded by the inverse matrix of the Chebyshev-VLM. Finally, after decoding and demodulation, the original information is obtained.

4. Simulation Results and Discussion

In the simulation, we use OQAM, where the size of the FFT/IFFT block is 128. The BER is tested by simulation experiments in a multipath channel.

Figure 3 shows the results for the clipping and filtering of FBMC signals, and the histograms as probability density functions (PDFs), and power spectra of the passband clipped signal $x_c^p[m]$ and its filtered signal $x_c^p[m]$. Figure 3 shows that the amplitude of the clipped signal is distributed below the clipping level. Finally, it can be seen from Fig. 3 that the filtered signal shows a peak value beyond the clipping level. It can also be seen that the OOB spectrum increases after clipping, but decreases again after filtering.

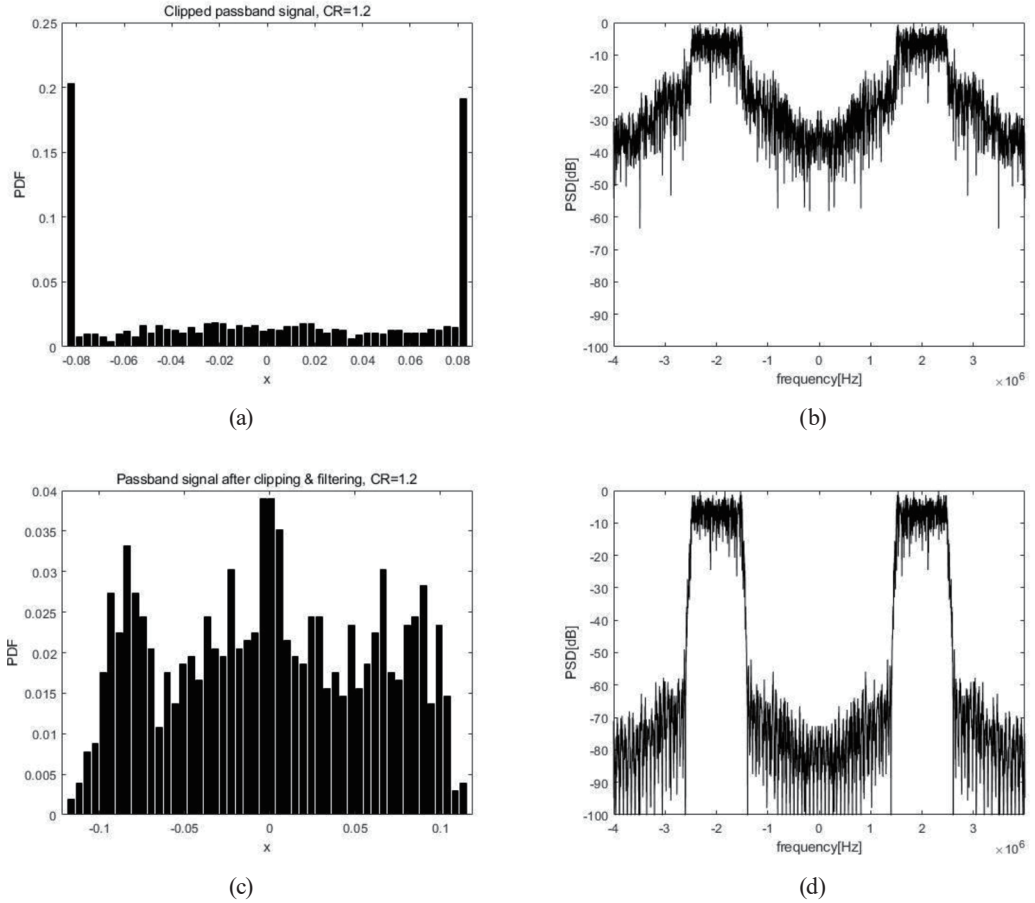

Fig. 3. Histograms (PDFs) and power spectra of FBMC signals with clipping and filtering (CR = 1.2).

Figure 4 shows the CCDFs of the crest factor for the clipped and filtered FBMC signals. The following are the parameters used for the simulation of clipping and filtering: 4-QAM signal constellation, N = 256 subcarriers, f = 1 MHz sampling frequency, and L = 8 oversampling factor. Recall that the CCDF of the crest factor can be considered to approximate the PAPR distribution since the crest factor is the square root of the PAPR. It can be seen from Fig. 4 that the PAPR of the FBMC signal decreases significantly after clipping and increases slightly after filtering. Note that the smaller the CR is, the greater the PAPR reduction effect is. Figure 5 shows the BER performance when the clipping and filtering technique is used. In Fig. 5, "C" and "C&F" denote the cases with clipping only and with both clipping and filtering, respectively.

Clipping also causes OOB radiation, which imposes OOB interference signals to adjacent channels. Although the OOB signals caused by clipping can be reduced by filtering, it may affect high-frequency components of the in-band signal (aliasing) when clipping is performed with the Nyquist sampling rate in the discrete-time domain. However, if clipping is performed for the sufficiently oversampled FBMC signals in the discrete-time domain before a low-pass filter (LPF) and the signal passes through a band-pass filter (BPF), the BER will be less degraded.

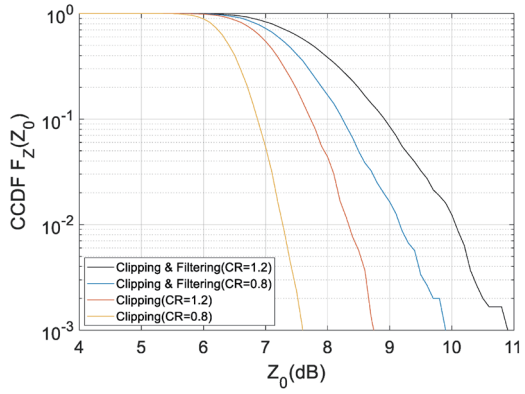

Fig. 4. (Color online) PAPR distribution with clipping and filtering.

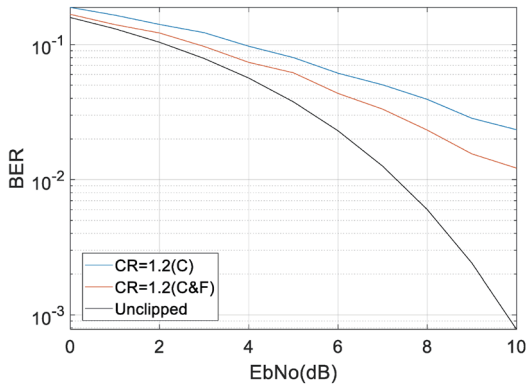

Fig. 5. (Color online) BER performance with clipping and filtering.

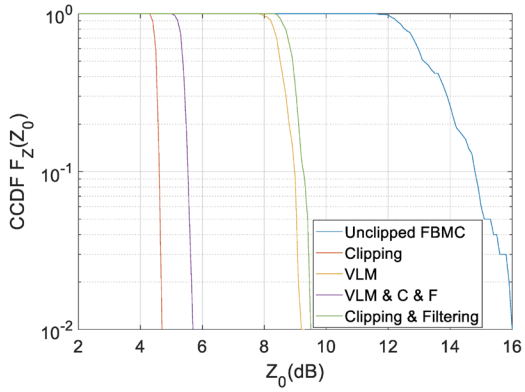

Fig. 6. (Color online) PAPR distribution with hybrid method.

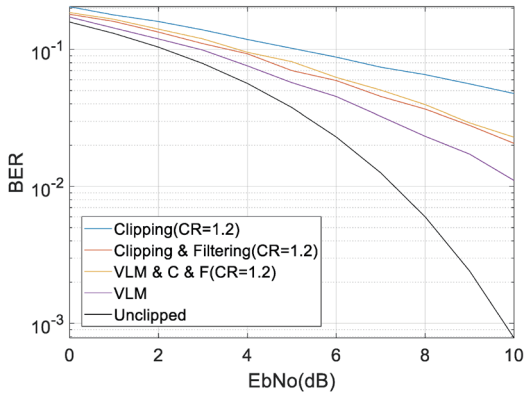

Fig. 7. (Color online) BER performance with hybrid method.

Figure 6 shows the PAPR performance when the VLM and clipping with filtering are used. It can be seen from this figure that when CCDF = 10^{-2}, the Z_0 values of clipping and VLM, clipping and filtering and VLM, VLM, and clipping and filtering are 4.4, 4.8, 8.6, and 8.8 dB, respectively. Compared with the VLM precoding method and clipping and filtering methods, the hybrid method can improve the PAPR suppression effect of the FBMC system. Figure 7 shows the BER performance when the VLM and clipping with filtering are used. It can be seen from this figure that the BER is highest when clipping is used only, and the BER decreases when clipping and filtering are used. Clipping causes in-band signal distortion, resulting in the BER performance degradation. Clipping also causes OOB radiation, which imposes OOB interference signals to adjacent channels. The OOB signals caused by clipping can be reduced by filtering. It can also be seen from this figure that the BER performance increases when the hybrid method is used. The VLM coding technique is used to select such codewords that minimize or reduce the PAPR. It causes no distortion and creates no OOB radiation.

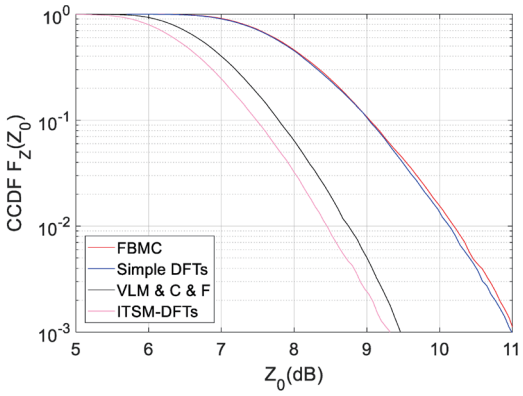

Fig. 8. (Color online) PAPR distribution with different schemes.

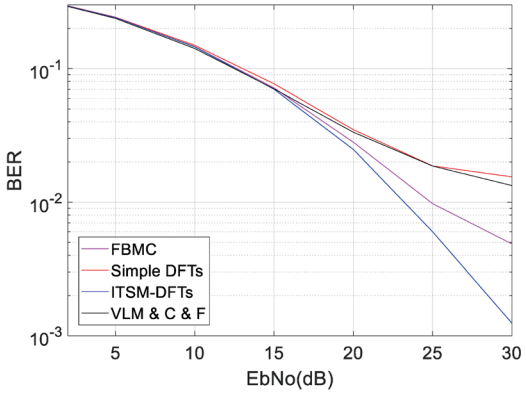

Fig. 9. (Color online) BER performance with different schemes.

Figure 8 shows the CCDF of the PAPR for a 4-QAM signal constellation and N = 256 subcarriers. The PAPR's CCDF curves of the pure FBMC and the DFT-spread schemes are also included for comparison. FBMC has the same PAPR as the simple DFT-spread FBMC. ITSM-DFT-spread FBMC[17] has the same PAPR as the hybrid method, but with an additional advantage of much lower OOB emission. Moreover, ITSM-DFT-spread FBMC is approximately 1.5 dB better than FBMC and the simple DFT-spread FBMC. This is because in addition to DFT spreading, ITSM-DFT-spread FBMC has another factor for further PAPR reduction, i.e., selection among the four waveform variations with different peak powers. Figure 9 shows the BER for a 16-QAM signal constellation, N = 256 subcarriers, F = 15 kHz subcarrier spacing, and f_c = 2.5 GHz carrier frequency. The simple DFT-spread FBMC has the same BER as the hybrid method. Only for high signal noise ratios, small deviations can be observed because the channel-induced interference is not Gaussian-distributed.

5. Conclusions

A hybrid method of VLM and clipping with filtering was applied to reduce the PAPR of pilot-assisted FBMC in WSNs. The correlation was reduced by the linear precoding of the encoded modulated data, and the PAPR of the FBMC signal was further reduced by clipping and filtering. From the simulation results, we observed that the hybrid method has a lower PAPR than the unclipped system and a lower BER than the case with clipping only. CR also affects the PAPR performance of the FBMC system: the smaller the CR is, the greater the PAPR reduction effect is.

References

1 D. M. Pham and S. M. Aziz: Object Extraction Scheme and Protocol for Energy Efficient Image Communication over Wireless Sensor Networks (Elsevier North-Holland, Inc., New York, 2013).
2 L. Feng: Telecommun. Network Technol. **5** (2015) 80.
3 F. Cruz-Roldán and M. Blanco-Velasco: Signal Process. **91** (2011) 1622.

4 B. Farhang-Boroujeny: IEEE Signal Process. Mag. **28** (2011) 92.
5 F. Cruz-Roldán, F. A. Pinto-Benel, J. D. O. del Campo, and M. Blanco-Velasco: J. Franklin Inst. **353** (2016) 1654.
6 J.-P. Javaudin, D. Lacroix, and A. Rouxel: 57th IEEE Vehicular Technology Conference (VTC) **3** (2003) 1581.
7 T. H. Stitz, T. Ihalainen, A. Viholainen, and M. Renfors: EURASIP J. Adv. Signal Process. **2010** (2010) 9.
8 R. Nissel and M. Rupp: IEEE Int. Conf. Acoustics, Speech and Signal Processing (ICASSP) (IEEE, 2016).
9 T. S. Mishmy and V. S. Sheeba: 3rd Int. Conf. Adv. Comput. Commun. (IEEE, 2013).
10 S. S. K. C. Bulusu, H. Shaiek, D. Roviras, and R. Zayani: Int. Wireless Communications Systems (IEEE, 2014).
11 A. Hanprasitkum, A. Numsomran, P. Boonsrimuang, and P. Boonsrimuang: Int. Conf. Advanced Communication Technology (IEEE, 2017).
12 D. Qu, S. Lu, and T. Jiang: IEEE Trans. Signal Process. **61** (2013) 1605.
13 N. Varghese, J. Chunkath, and V. S. Sheeba: 4th Int. Conf. Advances in Computing & Communications (IEEE, 2014).
14 H. Hrasnica, A. Haidine, and R. Lehnert: Broadband Powerline Communications: Network Design (Wiley, 2005).
15 M. Zimmermann and K. Dostert: IEEE Trans. Commun. **50** (2002) 553.
16 B. S. Krongold and D. L. Jones: IEEE Trans. Broadcasting **49** (2003) 258.
17 N. Dongjun and K. Choi: IEEE Trans. Wireless Commun. **99** (2017)1.
18 Hasan, Md. Mahmudul: Wireless Pers. Commun. **73** (2013) 791.

About the Authors

Song Liu received his B.S. degree from Shanghai Jiao Tong University, China, in 2000 and his M.S. and Ph.D. degrees from Waseda University, Japan, in 2004 and 2011, respectively. From 2010 to 2012, he was an assistant professor at Waseda University, Japan. Since 2012, he has been an associate professor at North China Electric Power University, China. His research interests are in smart energy system, electric data analysis, and broadband power line communication. (liusong@ncepu.edu.cn)

Yue Li received her B.S. degree from North China Electric Power University, China, in 2017. She is a graduate student and will receive her M.S. degree from North China Electric Power University, China, in 2020. Her research interests are in the physical layer for 5G communication systems and beyond. (liyue@ ncepu.edu.cn)

Jianqiang Wang received his B.S. and M.S. degrees from North China Electric Power University, China, in 2007 and 2012, respectively. Since 2012, he has been a senior engineer, deputy chief engineer, and director of the business office of the power marketing service and operation management branch at Inner Mongolia Power (Group) Co., Ltd. His research interests are in electric data analysis and wireless fading channels.
(wangjianqiang@ impc.com.cn)